BMC Medical Imaging

RESEARCH

Open Access

Application of deep learning reconstruction combined with time-resolved post-processing method to improve image quality in CTA derived from low-dose cerebral CT perfusion data

Jiajing Tong[1†], Tong Su[1†], Yu Chen[1*†], Xiaobo Zhang[1], Ming Yao[2], Yanling Wang[1], Haozhe Liu[1], Min Xu[3], Jian Wang[3] and Zhengyu Jin[1†]

Abstract

Background To assess the effect of the combination of deep learning reconstruction (DLR) and time-resolved maximum intensity projection (tMIP) or time-resolved average (tAve) post-processing method on image quality of CTA derived from low-dose cerebral CTP.

Methods Thirty patients underwent regular dose CTP (Group A) and other thirty with low-dose (Group B) were retrospectively enrolled. Group A were reconstructed with hybrid iterative reconstruction (R-HIR). In Group B, four image datasets of CTA were gained: L-HIR, L-DLR, L-DLR_{tMIP} and L-DLR_{tAve}. The CT attenuation, image noise, signal-to-noise ratio (SNR), contrast-to-noise ratio (CNR) and subjective images quality were calculated and compared. The Intraclass Correlation (ICC) between CTA and MRA of two subgroups were calculated.

Results The low-dose group achieved reduction of radiation dose by 33% in single peak arterial phase and 18% in total compared to the regular dose group (single phase: 0.12 mSv vs 0.18 mSv; total: 1.91mSv vs 2.33mSv). The L-DLR_{tMIP} demonstrated higher CT values in vessels compared to R-HIR (all $P<0.05$). The CNR of vessels in L-HIR were statistically inferior to R-HIR (all $P<0.001$). There was no significant different in image noise and CNR of vessels between L-DLR and R-HIR (all $P>0.05$, except $P=0.05$ for CNR of ICAs, 77.19 ± 21.64 vs 73.54 ± 37.03). However, the L-DLR_{tMIP} and L-DLR_{tAve} presented lower image noise, higher CNR (all $P<0.05$) and subjective scores (all $P<0.001$) in vessels than R-HIR. The diagnostic accuracy in Group B was excellent (ICC = 0.944).

†Jiajing Tong and Tong Su contributed equally to this work.

†Yu Chen and Zhengyu Jin contributed equally to this work.

*Correspondence:
Yu Chen
bjchenyu@126.com

Full list of author information is available at the end of the article

BMC

© The Author(s) 2025. **Open Access** This article is licensed under a Creative Commons Attribution-NonCommercial-NoDerivatives 4.0 International License, which permits any non-commercial use, sharing, distribution and reproduction in any medium or format, as long as you give appropriate credit to the original author(s) and the source, provide a link to the Creative Commons licence, and indicate if you modified the licensed material. You do not have permission under this licence to share adapted material derived from this article or parts of it. The images or other third party material in this article are included in the article's Creative Commons licence, unless indicated otherwise in a credit line to the material. If material is not included in the article's Creative Commons licence and your intended use is not permitted by statutory regulation or exceeds the permitted use, you will need to obtain permission directly from the copyright holder. To view a copy of this licence, visit http://creativecommons.org/licenses/by-nc-nd/4.0/.

Conclusion Combining DLR with tMIP or tAve allows for reduction in radiation dose by about 33% in single peak arterial phase and 18% in total in CTP scanning, while further improving image quality of CTA derived from CTP data when compared to HIR.

Keywords Computed tomography angiography, Deep learning, Cerebral arteries, Radiation dose reduction

Background

Computed tomography angiography (CTA) is widely utilized in diagnosing cerebrovascular diseases, particularly acute ischemic stroke and vascular malformations, due to its rapid and non-invasive features [1]. The emergence of dynamic CTA, also known as 4D-CTA, derived from whole-brain CT perfusion (CTP) data, holds great promise in vascular imaging by describing the dynamic assessment of contrast medium over time [2]. However, one significant drawback of 4D-CTA is the relatively high radiation dose associated with repeated scans, a practice not endorsed by the Food and Drug Administration, USA [3]. Consequently, various radiation reduction techniques have been proposed to address this issue, including adjustments to scanning parameters such as tube voltage, tube current, and sampling frequency [4]. Nevertheless, reducing radiation dose can lead to higher image noise and compromised image quality. Subsequently, methods to enhance image quality are introduced.

The advancement of image reconstruction algorithms can effectively reduce image noise and either maintain or enhance image quality in low-dose CT scans. The implementation of Hybrid Iterative Reconstruction (HIR), such as Adaptive Iterative Dose Reduction 3D (AIDR-3D), in CT imaging has demonstrated significant noise reduction benefits when compared to the conventional filtered back projection (FBP) reconstruction method [5, 6]. However, a notable limitation of HIR is its potential to overly smooth image appearance or texture [7]. Recently, with the rise of artificial intelligence, research efforts have shifted towards utilizing deep learning reconstruction (DLR) algorithms in medical imaging. Among the commercially available DLR algorithms, the Advanced Intelligent Clear-IQ Engine (AiCE), based on deep convolutional neural networks (DCNN), stands out for its ability to differentiate noise from true signal [8]. Images produced through DLR algorithms exhibit improved spatial resolution without compromising texture compared to HIR [9]. Numerous clinical studies have underscored the superior radiation exposure control and image quality achieved with DLR over unenhanced head CT [10, 11] and brain CTA scans [12].

In addition, significant advancements in post-processing method for perfusion CT have been proposed and validated to enhance image quality. Time-resolved CT is a sophisticated imaging technique that integrates data from multiple optimal time points to generate time-resolved maximum intensity projections (tMIP) or average intensity projections (tAve) image. By consolidating information from multiple images and incorporating noise reduction algorithms, this method has been demonstrated to significantly enhance image quality and diagnostic accuracy compared to conventional single-phase CTA [13, 14]. Various studies [2, 15] along with our own previous research [16] have demonstrated that time-resolved CTA images derived from cerebral CTP and reconstructed using HIR exhibit remarkable capabilities in visualizing vascular branches and anomalies. Nevertheless, to date, there has been a lack of research regarding the combination of this approach with DLR algorithms.

Our objective is to evaluate the impact of combining the DLR algorithm with the time-resolved CTA post-processing method on the image quality of CTA obtained from low-dose cerebral CTP, in comparison with HIR at standard dose levels.

Methods

Study population

This study was approved by the ethics committee (I-24PJ0479), and the requirement of informed consent was waived. A total of sixty consecutive patients were retrospectively enrolled. Group A (Regular dose) comprised 30 patients who underwent whole-brain dynamic CTP for ischaemic stroke between June 2020 and November 2020. Group B (Low dose) consisted of another 30 patients between January 2021 and December 2021. Patients with allergic action to iodine-containing contrast media, serve liver and kidney dysfunction, serve compensated cardiac insufficiency, pregnancy, and aged below 18 were excluded from the study.

CT acquisition

All CTP were performed with a 320 row-detector CT scanner (Aquilion ONE Genesis Edition, Canon Medical Systems, Japan). The patients were placed in the supine position with arms on the both sides of the body, and all were asked not to move during the examination. The scan was performed from atlas to cranial parietal in a caudocranial direction. Each patient was performed with a basic noncontrast CT and volumetric scanning for dynamic CTP with 19 phases: one noncontrast scan, three earlier arterial phase scans (interval 2 s), six arterial phase scans (interval 2 s), four late arterial phase scans (interval 2 s), and five venous phase scans (interval 5 s). The setting of tube current affecting radiation dose in these phases was summarized in Table 1. Other identical parameters between two groups were as follows: detector collimator = 320 × 0.5 mm; rotating speed = 0.5 s/r; and tube voltage = 80 kV. A total of 40 ml contrast media was injected into the median cubital vein at the rate of 5.0 ml/s by a power injector, and followed by 30 ml saline flush with same rate.

Image reconstruction and processing

The original image retrieved from Group A was reconstructed using HIR with clinically recommended setting [Adaptive Iterative Dose Reduction (AIDR-3D), kernel FC41]. The images from Group B were reconstructed using the same HIR setting as Group A, along with DLR using the Advanced Intelligent Clear-IQ Engine (AiCE) for Brain CTA.

All datasets were transferred to a professional workstation (Canon console, Canon Medical System, Japan) for imaging post-processing by one radiologist (three years of experience in the image diagnose of head and neck). The time attenuation curves of middle artery were separately generated for each dataset of two groups and the single arterial phase image derived from the time point with the best enhancement was extracted respectively (R-HIR, L-HIR, L-DLR). For the perfusion datasets reconstructed with DLR in Group B, time-resolved maximum intensity projection image (L-DLR_{tMIP}) and time-resolved average image (L-DLR_{tAve}) derived from three adjacent time points with the greatest enhancement and identical scan phase were obtained additionally. The L-DLR_{tMIP} and L-DLR_{tAve} images were generated using the vendor's software (tMIP and tAve) installed in the CT console, where the registration process for motion correction was integrated. Then five image sets (R-HIR, L-HIR, L-DLR, L-DLR_{tMIP}, L-DLR_{tAve}) from two groups were reconstructed with a thickness of 0.5 mm, slice interval of 0.5 mm, and pixel matrix of 512 × 512 for the subsequent analysis.

Image analysis

Objective image analysis

A radiologist with 3 years of experience in head and neck imaging performed the quantitative analysis and calculated the mean CT attenuation values, image noise, signal-to-noise ratio (SNR), and contrast-to noise ratio (CNR) at the same position of each image. The regions of interest (ROIs) were placed in the siphon segment of bilateral internal carotid arteries (ICAs), middle cerebral arteries (MCAs), basilar artery (BA), and brainstem (BS). And the ROIs were set as large as possible while avoiding the artifacts and arterial calcifications (Fig. 1). The attenuation values in the vessel (CT_{vessel}) were calculated as the average of the measurements in the center of each artery (BA, ICAs, MCAs). The image noise was defined as the standard deviation (SD) of the brainstem attenuation measurements. For each of the image sets, the calculations of SNR and CNR were performed as follows:

$$\mathrm{SNR_{ROI}} = \mathrm{CT_{ROI}}/\mathrm{SD_{ROI}}$$

$$\mathrm{CNR_{vessel}} = (\mathrm{CT_{vessel}} - \mathrm{CT_{brainstem}})/\mathrm{SD_{brainstem}}$$

Table 1 CTP tube current of Group A and Group B

	Group A	Group B
Noncontrast phase (1 scan)	300 mA	200 mA
Earlier arterial phase (3 scans)	150 mA	150 mA
Arterial phase (6 scans)	300 mA	200 mA
Later arterial phase (4 scans)	150 mA	150 mA
Venous phase (5 scans)	150 mA	150 mA

Subjective image analysis

All images were independently and subjectively evaluated by two radiologists (with 10 and 3 years of experience in CTA of head and neck), who were blinded to the scanning parameters and the reconstruction methods. The window width and window level setting having influence on image quality were consistent in all datasets. Sagittal thin-slab maximum intensity projection (MIP) images were reconstructed for five sets and presented in random order. Overall image quality was evaluated using a 5-point scale with respect to clarity of small vessels and noise: 5 = excellent image quality, distal second-order branches visualized with little image noise; 4 = good image quality, second-order branches completely visualized with little image noise; 3 = moderate image quality, second-order branches not completely visualized with average image noise; 2 = nondiagnostic image quality, first-order branches clearly visualized with significant image quality; 1 = poor image quality, main branches not completely visualized with significant image noise. Figure 2 showed the images with different scores.

Arterial stenosis

Only patients underwent both CTP and MRA were performed the analysis of arterial stenosis, therefore only a subgroup of patients was included. The MRA was performed on a 3.0 T MR imaging system (Signa General, electric medical system, Milwankee, WI, USA) with 3D TOF technique. The image parameters were as follow: angle, 20°; echo time/repetition time: 39/2.6 ms. Images were set to workstation for post-processing to punch veins, isolate anterior and posterior circulation arteries, and create 12 MIP images that were radially projected at 15-degree increments. Then the CTA and MRA data were evaluated by two well-experienced radiologist mentioned above, who were blinded to the patients' information and reached a consensus conclusion. Intracranial arteries were divided into 21 segments, including bilateral C2-7

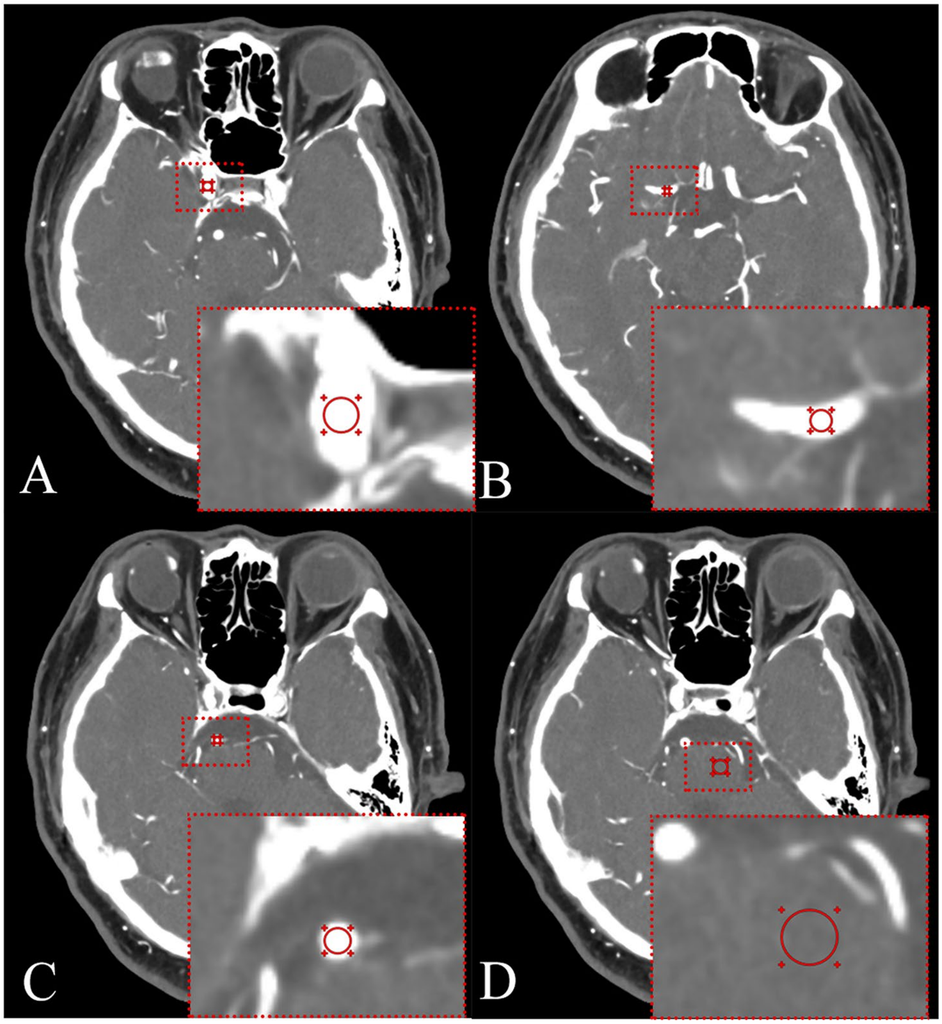

Fig. 1 ROIs of objective image quality evaluation. The regions of interest (ROIs) were placed in the siphon segment of bilateral internal carotid arteries (**A**), middle cerebral arteries (**B**), basilar artery (**C**), and brainstem (**D**)

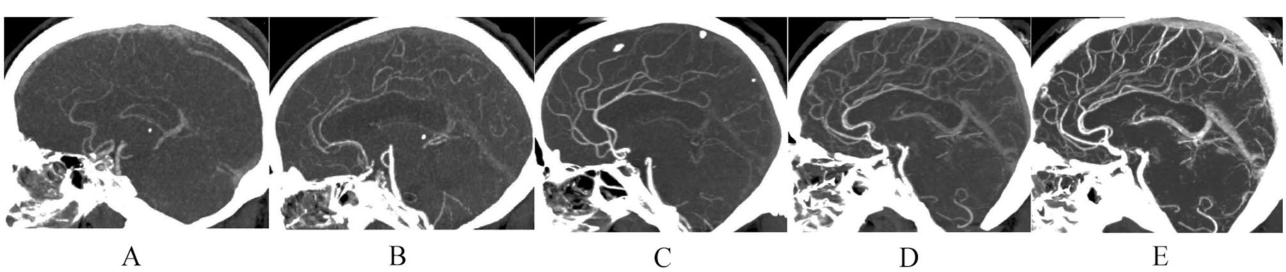

Fig. 2 Subjective image quality criteria graded on 5-point scale (5 = excellent, 1 = poor). **A** image quality of score 1 (main branches not completely visualized with significant image noise). **B** image quality of score 2 (first-order branches clearly visualized with significant image quality). **C** image quality of score 3 (second-order branches not completely visualized with average image noise). **D** image quality of score 4 (second-order branches completely visualized with little image noise). **E** image quality of score 5 (distal second-order branches visualized with little image noise)

segments of the ICA, bilateral anterior cerebral artery (ACA), bilateral middle cerebral artery (MCA), bilateral posterior cerebral artery (PCA), bilateral V4 of the vertebral artery (VA) and BA. A 4-point scale according to the North American Symptomatic Carotid Endarterectomy Trial criteria [17] was used to evaluated the arteries and explained as follows: 0 = non stenosis (0%), 1 = mild stenosis (<50%), 2 = moderate stenosis (50%-69%), 3 = severe stenosis (70%-99%), and 4 = complete occlusion (100%).

Radiation dose

The CT dose index volume ($CTDI_{vol}$) and dose length product (DLP) were automatically recorded for each phase. The efficient dose (ED) was calculated using DLP multiplied by a conversion coefficient k factor of 0.0021 ($mSv•mGy^{-1}•cm^{-1}$) [18]. To make the difference more clear between two groups, the radiation dose of single arterial phase was calculated additionally.

Statistical analysis

Continuous variables were expressed as mean ± standard deviation or median and interquartile range, depending on the normality of the data assessed by The Shapiro-Wilk test. For the comparisons of CT value, image noise, SNR, and CNR between two groups, t test (for normally distributed data) or Wilcoxon-Mann-Whitney (for non-normally distributed data) was employed. For the evaluation of subjective image quality, interreader reliability was assessed using weighted kappa statistics and interpreted as follows: poor (ĸ = 0-0.20), fair (ĸ = 0.21–0.40), moderate (ĸ = 0.41–0.60), good (ĸ = 0.61–0.80), and excellent (ĸ = 0.81–1.00). For the evaluation of Arterial stenosis, The Intraclass Correlation (ICC) between CTA and MRA of two groups were calculated. Statistical analysis was performed using R software (version 3.6.1, http://www.R-project.org). $P < 0.05$ was considered statistically significant in difference.

Results

Patient population and radiation dose

The patient characteristics, including age, gender, weight, and body mass index (BMI), of each group were summarized in Table 2. No statistically significant differences in patient characteristics were found between the two groups (all $P > 0.05$). In single arterial phase of Group A, The DLP was 85.3 mGy·cm, the $CTDI_{vol}$ was 5.3 mGy and the ED was 0.18 mSv. The total $CTDI_{vol}$ for a CTP scan in Group A was 1108.3 mGy, with a total ED of 2.33 mSv. In single arterial phase of Group B, The DLP was 56.8 mGy·cm, the $CTDI_{vol}$ was 3.6 mGy and the ED was 0.12 mSv. The total $CTDI_{vol}$ for a CTP scan in Group B was 908.8 mGy and total ED was 1.91 mSv.

Objective image analysis

The comparison of objective image quality between Group A and Group B is presented in Table 3. The L-DLR_{tMIP} demonstrated higher CT values in ICAs, MCAs and BA compared to R-HIR (all $P < 0.05$). There were no significant differences in CT attenuation of the vessels when comparing L-HIR, L-DLR and L-DLR_{tAve} to R-HIR (all $P > 0.05$, except $P = 0.05$ for L-HIR and R-HIR in ICAs: 619.88 ± 144.06 vs 702.72 ± 167.65). The SD and SNR of all vessels in L-HIR, L-DLR, L-DLR_{tMIP} and L-DLR_{tAve} were inferior to that of R-HIR (all $P < 0.05$). Notably, the SD of the brainstem in L-HIR was higher than that in R-HIR ($P < 0.001$), while there was no statistically significant difference between L-DLR and R-HIR ($P = 0.28$). However, L-DLR_{tMIP} and L-DLR_{tAve} exhibited lower image noise than R-HIR ($P \leq 0.001$), resulting in a higher CNR for vessels by approximately 31–38% and 43–55% respectively (Fig. 3).

Table 2 Characteristics of the study population

	Group A (n = 30)	Group B (n = 30)	*P*-value
Age, years	57.67 ± 17.89	56.00 ± 17.51	0.72
Males, n	20 (66.7%)	17 (56.7%)	0.43
Weight, kg	68.10 ± 13.15	66.42 ± 13.95	0.63
BMI, kg/m^2	24.97 ± 3.83	23.82 ± 3.81	0.25

Subjective image analysis

The inter-reader reliability was excellent (ĸ = 0.81). All images reconstructed with DLR (L-DLR, L-DLR_{tMIP} and L-DLR_{tAve}) showed higher scores and superior image quality compared to R-HIR (all $P < 0.001$), while the score of L-HIR was lower than of R-HIR ($P < 0.05$). The detailed results of subjective analysis are summarized in Table 4.

Diagnostic accuracy of stenosis

MRA was conducted on 8 patients, with 5 in Group A and 3 in Group B, encompassing a total of 168 arterial segments (105 in Group A, 63 in Group B) in this study. The average time interval between CTP and MRA was 58.8 days in Group A (115, 85, 19, 5, 70 days respectively) and 11 days in Group B (20, 11, 2 days respectively). Using MRA results as the reference standard, in Group A, 81% of arterial segments (85/105) were classified as normal, 16% (17/105) with mild stenosis, 2% (2/105) with moderate stenosis, 1% (1/105) with severe stenosis, and no complete arterial occlusion. Group B exhibited 57% of arterial segments (36/63) classified as normal, 32% (20/63) with mild stenosis, 3% (2/63) with moderate stenosis, 8% (5/63) with complete occlusion, and no segments with severe stenosis. For Group B, the evaluated results were consistent across all four CTA images, leading to the calculation of the ICC between MRA and CTAs in Group B only once. The ICC was 0.896 (95%CI: 0.851, 0.928) in Group A and 0.761 (95%CI: 0.634, 0.849) in Group B. An interesting observation was made in one patient from Group B, where the bilateral posterior cerebral arteries were completely occluded in MRA but showed normal or mild stenosis in CTA. Consequently, a second ICC calculation excluding these two arterial segments was performed, yielding a higher ICC of 0.944 (95%CI: 0.903, 0.967) after their exclusion.

Table 3 Objective assessment of image quality

		R-HIR	L-HIR	L-DLR	L-DLR$_{tMIP}$	L-DLR$_{tAve}$	R-HIR vs. L-HIR	R-HIR vs. L-DLR	R-HIR vs. L-DLR$_{tMIP}$	R-HIR vs. L-DLR$_{tAve}$
CT	ICAs	702.72 (167.65)	619.88 (144.06)	759.10 (193.51)	823.1 (210.08)	707.25 (176.66)	0.05	0.09	0.003	0.56
	MCAs	657.18 (162.78)	605.21 (129.82)	739.13 (183.32)	754.35 (179.45)	678.81 (165.15)	0.26	0.06	0.03	0.33
	BA	643.86 (163.33)	539.20 (142.49)	666.02 (196.99)	739.14 (176.30)	623.15 (166.03)	0.12	0.65	0.04	0.64
	BS	51.90 (5.06)	54.76 (5.22)	46.15 (5.36)	52.61 (4.59)	45.50 (4.83)	0.04	<0.001	0.58	<0.001
SD	ICAs	10.24 (3.80)	28.68 (15.97)	39.91 (21.57)	39.09 (22.19)	32.39 (20.14)	<0.001	<0.001	<0.001	<0.001
	MCAs	10.31 (4.47)	24.99 (9.85)	25.19 (10.27)	26.11 (12.69)	17.83 (9.36)	<0.001	<0.001	<0.001	0.002
	BA	10.23 (5.08)	43.87 (19.14)	42.00 (20.38)	46.44 (19.21)	39.08 (16.20)	<0.001	<0.001	<0.001	<0.001
	BS	10.09 (3.20)	14.30 (1.63)	9.39 (1.35)	7.70 (1.45)	6.07 (1.10)	<0.001	0.28	0.001	<0.001
SNR	ICAs	81.09 (45.15)	27.26 (13.66)	24.73 (12.49)	26.24 (12.36)	28.97 (15.97)	<0.001	<0.001	<0.001	<0.001
	MCAs	82.26 (52.88)	27.59 (11.77)	32.54 (12,01)	33.69 (12.27)	45.43 (18.07)	<0.001	<0.001	<0.001	<0.001
	BA	79.62 (42.84)	14.59 (8.06)	19.57 (13.20)	17.79 (7.34)	20.02 (13.07)	<0.001	<0.001	<0.001	<0.001
	BS	5.72 (2.12)	3.87 (0.48)	5.00 (0.82)	7.00 (1.12)	7.65 (1.22)	<0.001	0.62	0.002	<0.001
CNR	ICAs	73.54 (37.03)	40.03 (10.61)	77.19 (21.64)	101.43 (25.42)	110.66 (29.69)	<0.001	0.05	<0.001	<0.001
	MCAs	68.51 (35.08)	38.80 (9.65)	76.11 (21.38)	93.22 (25.13)	106.19 (24.55)	<0.001	0.09	0.002	<0.001
	BA	67.45 (36.10)	34.32 (10.22)	66.95 (21.34)	88.76 (24.39)	96.55 (27.46)	<0.001	0.38	0.001	<0.001

BA, basilar artery; BS, brainstem; CNR, contrast-to-noise ratio; DLR, Deep learning reconstruction; HIR, Hybrid iterative reconstruction; ICAs, internal carotid arteries; SNR, signal-to-noise ratio; tAve, time-resolved average; tMIP, time-resolved maximum intensity projection

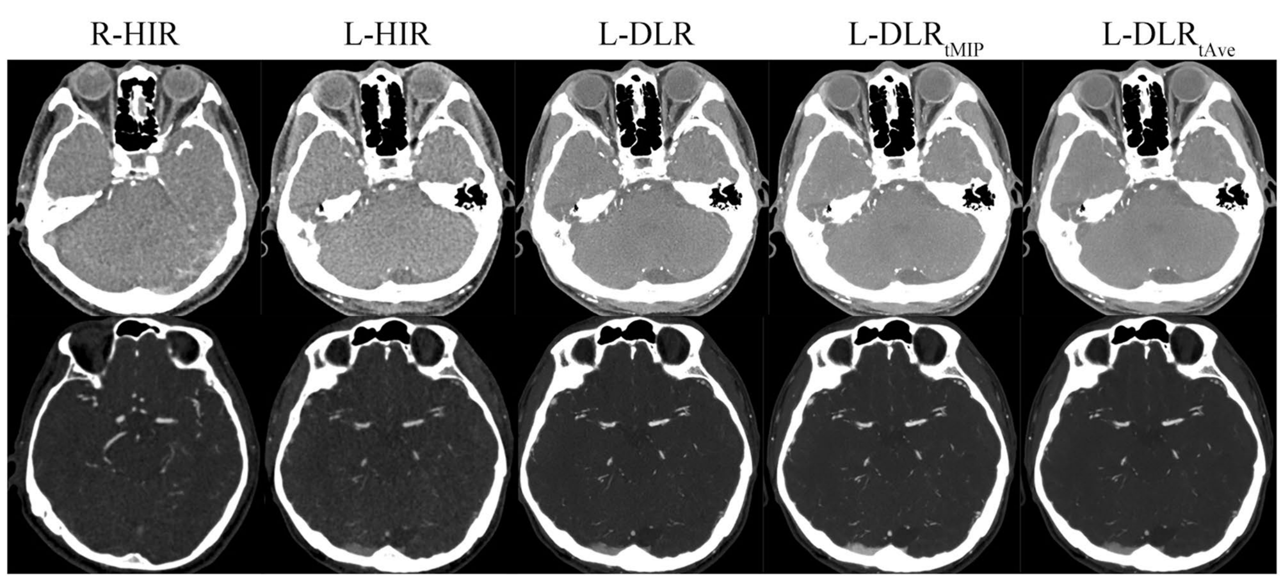

Fig. 3 Example demonstrating the impact of the different reconstruction methods of the brainstem with a window setting of the tissue (width 400HU, level 40HU) and middle arterial with a window setting of the vessel (width 1000HU, level 400HU)

Table 4 Subjective assessment of image quality

	R-HIR	L-HIR	L-DLR	L-DLR$_{tMIP}$	L-DLR$_{tAve}$	R-HIR vs. L-HIR	R-HIR vs. L-DLR	R-HIR vs. L-DLR$_{tMIP}$	R-HIR vs. L-DLR$_{tAve}$
Reader 1	4.20 (0.66)	3.80 (0.55)	4.77 (0.50)	4.87 (0.35)	4.90 (0.31)	0.02	<0.001	<0.001	<0.001
Reader 2	4.33 (0.66)	4.03 (0.41)	4.93 (0.25)	4.93 (0.25)	4.93 (0.25)	0.03	<0.001	<0.001	<0.001

DLR, Deep learning reconstruction; HIR, Hybrid iterative reconstruction; tAve, time-resolved average; tMIP, time-resolved maximum intensity projection

Discussion

In this study, we assessed the application of deep learning reconstruction algorithm and the time-resolved post-processing method in CTA images derived from low-dose cerebral CTP data by comparing the image quality with regular dose images reconstructed with HIR. Our results indicated that the combination of these two techniques could further enhance image quality, despite a significant reduction of 33% in radiation dose compared with R-HIR.

Recently years, several studies have validated the positive effect of DLR algorithm on image noise reduction and image quality improvement in low-dose scanning, including head CT [10], coronary CTA [19], chest CT [20], CT pulmonary angiography [21] and abdominal CT [22]. For instance, in non-contrast head CT [10], DLR presented lower image noise, higher gray matter-white matter contrast, and higher CNR than HIR even at 25% reduced dose setting. However, the potential of DLR algorithm for radiation reduction is limited. In a liver CT study by Lyu et al [23], where DLR was evaluated at different lower radiation dose levels against full-dose HIR, DLR's performance was subpar to full-dose HIR when at dose reductions exceeding 50%. Our study also found that L-DLR (33% dose reduction) exhibited inferior SD and SNR for vessels compared to R-HIR, while the CNR of vessels showed no significant difference (except ICAs). As a result, we considered to explore the feasibility of integrating DLR with other methodologies to further enhance image quality in low-dose settings.

Based on relevant literature in time-resolved CTA [16, 24, 25], post-processing is typically conducted at three time points. In our previous study [16], we had compared the objective and subjective image quality among HIR$_{tMIP}$, HIR$_{tAve}$ and HIR$_{peak}$ in 4D-CTA, and concluded that time-resolved CTA was preferred to visualize vascular branches when at the same dose level. Building on this, we further assessed the impact of the combination of DLR and tMIP or tAve based on the three adjacent time points with the greatest enhancement at lower dose level. Our results found that L-DLR with tMIP and tAve achieved enhanced CNR of all vessels approximately 31–38% and 43–55%, respectively, compared to images obtained with HIR at regular dose. This result suggested that the combination outperformed using DLR alone and demonstrated the feasibility of enhancing noise reduction and improving objective image quality in 4D-CTA scans with a 33% lower dose by integrating the DLR algorithm with time-resolved CTA post-processing methods.

Subjectively, a previous study [12] had shown the advantage of DLR over FBP and HIR at the same dose level in depicting small intracranial vessels. This was attributed to DLR's ability to enhance spatial resolution and depict small cortical branches effectively. Our study was consistent with that. As illustrated in Figure 4–5, the visualization of distal second-order branches was notably clearer with DLR compared to HIR, irrespective of whether time-resolved post-processing methods were combined or not. This indirectly reflected the enhanced spatial resolution of DLR as higher spatial resolution allows for better visualization of small anatomical structures and results in higher subjective scores. What set our study apart was the observed enhancement when comparing low-dose DLR images to regular-dose HIR images. Therefore, our result further validated the benefit of DLR in small intracranial vessels depiction in 4D-CTA scan when implementing 33% dose reduction.

In the assessment of arterial stenosis, MRA was found to grade two arterial segments as occluded, primarily due to overestimation issues [26]. This overestimation can be attributed to intravoxel dephasing and local signal loss resulting from flow velocity gradients, acceleration, and complex flow patterns encountered in MRA imaging. As it shows in Fig. 6, the bilateral posterior cerebral arteries were not visualized in the MRA image but were clearly delineated in the CTA images. In the case of this patient, the bilateral V4 segments of the VA, the proximal and mid BA were completely occluded, leading to slow flow velocities in the distal vessels that were challenging to image using MRA. Actually, the bilateral posterior cerebral arteries and distal BA were primarily supplied by the anterior circulation and the lumen was normal or mild stenosis. After excluding these two segments, the ICC in Group B was 0.944, compared to 0.896 in Group A. Consequently, the diagnostic accuracy achieved with low-dose DLR imaging (with or without the use of time-resolved post-processing methods) was comparable to, if not better than, that obtained with regular-dose HIR imaging.

In this study, we found the subjective image quality and diagnostic accuracy of arterial stenosis in the low-dose group (with a 33% reduction) using DLR alone were

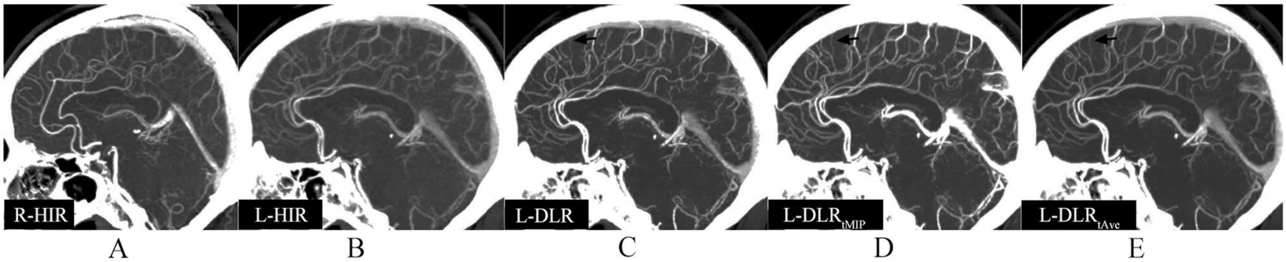

Fig. 4 An example of subjective score for image quality. Sagittal thin-slab maximum intensity projection (MIP) images were reconstructed. **A** A patient performed with R-HIR scan and the score is 4. **B–E** Another patient performed with L-HIR, L-DLR, L-DLR$_{tMIP}$ and L-DLR$_{tAve}$ scans. The scores are 4, 5, 5 and 5 respectively. The distal second-order branches are visualized clearer than HIR in the images with DLR, whether time-resolved post-processing method combined or not

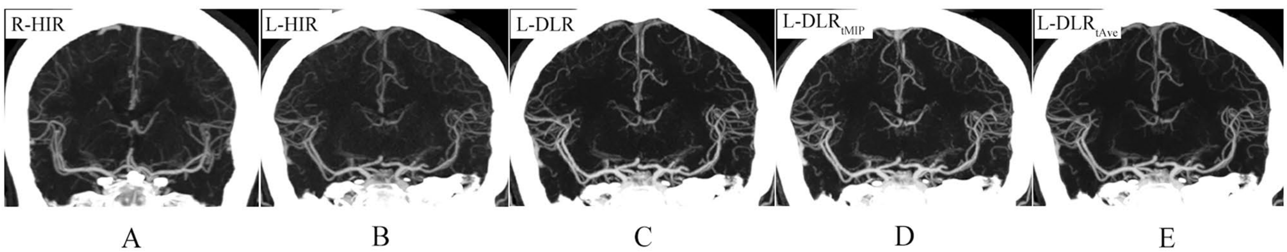

Fig. 5 Example of middle cerebral arteries. A 68-year old man in Group A was reconstructed with HIR (**A**). A 56-year-old man in Group B was reconstructed with HIR (**B**), DLR (**C**), DLR$_{tMIP}$ (**D**) and DLR$_{tAve}$ (**E**), there were no stenosis in the bilateral middle arteries. The vascular edge in images reconstructed with DLR (**C**–**E**) was sharper and clearer than those reconstructed with HIR (**A, B**)

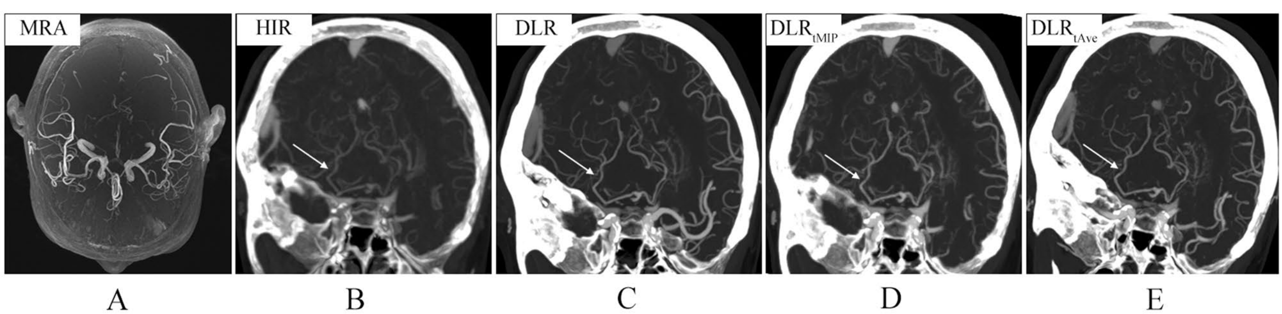

Fig. 6 Images of the excluded case in assessment of diagnostic accuracy of stenosis.A patient with occlusive bilateral V4 segments of the vertebral artery (VA), the proximal and mid based artery (BA). **A** The posterior circulation was not show in Maximum intensity projection (MIP) of MRA and included vessels (bilateral posterior cerebral artery, bilateral V4 of the VA and BA) were evaluated as occlusion. **B–E** Thin-MIP of CTA reconstructed by four methods (HIR, DLR, DLR$_{tMIP,}$ DLR$_{tAve}$) from CTP image sets showed distal BA and bilateral posterior cerebral artery clearly, and the arteries above were regarded as non or mild stenosis

superior to or on par with the results obtained from the regular dose group using HIR. The objective image quality could potentially be further improved to exceed the levels achieved with the regular dose by incorporating a time-resolved post-processing method. However, the potential advantages of this combination were somewhat tempered by the time-consuming nature of reconstructing these two elements in routine 4D-CTA scans, and there was no significant breakthrough in terms of diagnostic accuracy due to the limited number of cases. Consequently, the integration of the time-resolved method may be worth considering in specific challenging scenarios, such as when there is a need to highlight certain details in low-dose 4D-CTA scans that may not have been satisfactorily captured with DLR alone.

There were several limitations in this study. Firstly, all results and findings were derived from a relatively small sample size, particularly in terms of the number of patients who underwent DSA. Secondly, the benefit of spatial resolution provided by DLR was assessed indirectly through subjective evaluation in our study. Future research for a comprehensive evaluation should include objective assessment of spatial resolution. Thirdly, the diagnostic accuracy of DLR and DLR combined with a time-resolved post-processing method was assessed against the diagnostic results of MRA, as there was no gold standard examination (such as DSA) available. This reliance on MRA as the reference point may have introduced some uncertainty into the evaluation of arterial stenosis. Therefore, future studies should involve a larger cohort of patients who have undergone DSA to provide a more reliable assessment of diagnostic accuracy in arterial stenosis. Additionally, we compared CTA_{tMIP} and CTA_{tAve} using only the three time points with the highest enhancement, future studies will focus on determining the optimal combining post-processing strategy for various scenarios. Last but not least, the majority of patients included in this study were diagnosed with mild narrowing, and there was an imbalance in the distribution of narrowing degrees and the time intervals between CTP and MRA in the two groups. To address this issue, future research should incorporate a matched-pairs design and encompass a more comprehensive range of narrowing degrees for a more robust investigation.

Conclusions

In conclusion, the combination of DLR with time-resolved CTA post-processing method in CTA derived from low-dose cerebral CTP data (with a 33% reduction in a single peak arterial phase dose and an 18% reduction in total dose) significantly enhanced both the objective and subjective image quality of the vessels.

Abbreviations

HIR	Hybrid iterative reconstruction
DLR	Deep learning-based reconstruction
Tmip	Time-resolved maximum intensity projection
tAve	Time-resolved average
CTDIvol	CT dose index volume
DLP	Dose-length product
ED	Effective dose
BA	Basilar artery
BS	Brainstem

Acknowledgments

Not applicable.

Author contributions

Y.C. and Z.J. conceived the study. Y.C., X.Z., M.Y. and Z.J. designed the network. J.T., Y.W. and H.L. implemented the methods. J.T., T.S. M.X. and J.W. contributed to the image and statistical analysis. J.T., T.S. M.X. and Y.C. drafted the manuscript and contributed to the review and editing. All authors approved the manuscript.

Funding

This work was supported by the National Natural Science Foundation of China (grant number. 82001814) and the National High Level Hospital Clinical Research Funding (grant number. 2022-PUMCH-B-068).

Data availability

The datasets generated or analyzed during the study are available from the corresponding author on reasonable request.

Declarations

Ethics approval and consent to participate

Approval was granted by the ethics committee of Peking Union Medical College Hospital, Chinese Academy of Medical Sciences and Peking Union Medical College (Ethics approval number: I-24PJ0479), which agreed to waive informed consent due to the retrospective nature of this study. All methods were carried out in accordance with the Declaration of Helsinki.

Consent for publication

Not applicable.

Competing interests

The authors declare no competing interests.

Author details

[1]Department of Radiology, Peking Union Medical College Hospital, Chinese Academy of Medical Sciences & Peking Union Medical College, No.1 Shuaifuyuan, Dongcheng District, Beijing 100730, China
[2]Department of Neurology, Peking Union Medical College Hospital, Chinese Academy of Medical Sciences & Peking Union Medical College, No.1 Shuaifuyuan, Dongcheng District, Beijing 100730, China
[3]Canon Medical Systems (China), Building 205, Yard No. A 10, JiuXianQiao North Road, Chaoyang District, Beijing 100015, China

Received: 11 August 2024 / Accepted: 3 March 2025
Published online: 29 April 2025

References

1. Kortman HGJ, Smit EJ, Oei MTH, et al. 4D-CTA in neurovascular disease: a review. AJNR Am J Neuroradiol. 2015;36:1026–33.
2. Smit EJ, Vonken E, van der Schaaf IC, et al. Timing-invariant reconstruction for deriving high-quality CT angiographic data from cerebral CT perfusion data. Radiology. 2012;263:216–25.
3. Ringelstein A, Lechel U, Fahrendorf DM, et al. Radiation exposure in perfusion CT of the brain. J Comput Assist Tomogr. 2014;38:25–28.
4. Othman AE, Afat S, Brockmann MA, et al. Radiation dose reduction in perfusion CT imaging of the brain: a review of the literature. J Neuroradiol. 2016;43:1–5.
5. den Harder AM, Willemink MJ, de Ruiter QMB, et al. Achievable dose reduction using iterative reconstruction for chest computed tomography: a systematic review. Eur J Radiol. 2015;84:2307–13.
6. Mello-Amoedo CD de, Martins AN, Tachibana A, et al. Comparison of radiation dose and image quality of abdominopelvic CT using iterative (AIDR 3D) and conventional reconstructions. AJR Am J Roentgenol. 2018;210:127–33.
7. Mileto A, Guimaraes LS, McCollough CH, et al. State of the Art in Abdominal CT: the Limits of Iterative Reconstruction Algorithms. Radiology. 2019;293:491–503.
8. Arndt C, Güttler F, Heinrich A, et al. Deep Learning CT Image Reconstruction in Clinical Practice. Rofo. 2021;193:252–61.
9. Singh R, Wu W, Wang G, et al. Artificial intelligence in image reconstruction: the change is here. Phys Med. 2020;79:113–25.
10. Nagayama Y, Iwashita K, Maruyama N, et al. Deep learning-based reconstruction can improve the image quality of low radiation dose head CT. Eur Radiol. 2023;33:3253–65.
11. Altmann S, Abello Mercado MA, Ucar FA, et al. Ultra-high-resolution CT of the head and neck with deep learning reconstruction-assessment of image quality and radiation exposure and intraindividual comparison with normal-resolution CT. Diagnostics (Basel). 2023;13:1534.
12. Otgonbaatar C, Ryu J-K, Kim S, et al. Improvement of depiction of the intracranial arteries on brain CT angiography using deep learning reconstruction. J Integr Neurosci. 2021;20:967–76.
13. Brehmer K, Brismar TB, Morsbach F, et al. Triple Arterial Phase CT of the Liver with Radiation Dose Equivalent to That of Single Arterial Phase CT: initial Experience. Radiology. 2018;289:111–18.
14. Fischer MA, Leidner B, Kartalis N, et al. Time-resolved computed tomography of the liver: retrospective, multi-phase image reconstruction derived from volumetric perfusion imaging. Eur Radiol. 2014;24:151–61.

15. Willems PWA, Taeshineetanakul P, Schenk B, et al. The use of 4D-CTA in the diagnostic work-up of brain arteriovenous malformations. Neuroradiology. 2012;54:123–31.
16. Chen Y, Wang Y, Su T, et al. Deep learning reconstruction improves the image quality of CT angiography derived from 80-kVp cerebral CT perfusion data. Acad. Radiol. 2023;30:2666–73.
17. Huang J, Degnan AJ, Liu Q, et al. Comparison of NASCET and WASID criteria for the measurement of intracranial stenosis using digital subtraction and computed tomography angiography of the middle cerebral artery. J Neuroradiol. 2012;39:342–45.
18. Christner JA, Kofler JM, McCollough CH. Estimating effective dose for CT using dose-length product compared with using organ doses: consequences of adopting International Commission on Radiological Protection publication 103 or dual-energy scanning. AJR Am J Roentgenol. 2010;194:881–89.
19. Wang M, Fan J, Shi X, et al. A deep-learning reconstruction algorithm that improves the image quality of low-tube-voltage coronary CT angiography. Eur J Radiol. 2022;146:110070.
20. Jiang B, Li N, Shi X, et al. Deep Learning Reconstruction Shows Better Lung Nodule Detection for Ultra-Low-Dose Chest CT. Radiology. 2022;303:202–12.
21. Qiu SM, Zhang H, Liu ZX, et al. The application value of deep learning image reconstruction on improving image quality and evaluating the Qanadli embolism index of dual low-dose CT pulmonary angiography. Zhonghua Yi Xue Za Zhi. 2023;103:1477–82.
22. Xu JJ, Lönn L, Budtz-Jørgensen E, et al. Evaluation of thin-slice abdominal DECT using deep-learning image reconstruction in 74 keV virtual monoenergetic images: an image quality comparison. Abdom Radiol (NY). 2023;48:1536–44.
23. Lyu P, Liu N, Harrawood B, et al. Is it possible to use low-dose deep learning reconstruction for the detection of liver metastases on CT routinely? Eur Radiol. 2022;33:1629–40.
24. Yang L, Zhang H, Sheng J, et al. Contrast enhancement boost improves the image quality of CT angiography derived from 80-kVp cerebral CT perfusion data. BMC Med Imaging. 2024;24:193.
25. Liao K, Ye B, Li X, et al. Clinical application of third-generation dual-source CT-based dynamic imaging reconstruction for pulmonary embolism imaging. J Cardiothorac Surg. 2025;20:86.
26. Nederkoorn PJ, Elgersma OEH, WPThM M, et al. Overestimation of carotid artery stenosis with magnetic resonance angiography compared with digital subtraction angiography. J Vascular Surg. 2002;36:806–13.

Publisher's Note

Springer Nature remains neutral with regard to jurisdictional claims in published maps and institutional affiliations.